



Article

A Protection System for Improved Ring-Bus DC Microgrids

Zhiming Zhang ¹, Qing Chen ^{1,*}, Ranran Xie ² and Yi Zheng ³

¹ Key Laboratory of Power System Intelligent Dispatch and Control, Shandong University, Ministry of Education, Jinan 250061, China

² State Grid TianJin BinHai Electric Power Supply Company, Tianjin 300450, China

³ State Grid Jining Power Supply Company, Jining 272000, China

* Correspondence: qchen@sdu.edu.cn

Received: 30 August 2019; Accepted: 29 September 2019; Published: 4 October 2019



Abstract: An improved system structure and a corresponding protection system are proposed in this paper, which aims at providing future DC microgrids with suitable protection ideas. At first, the ring-bus system is adjusted to balance the system control and protection and make the system more conventional for the equipment expansion. In addition, based on this structure, a protection system is established. It consists of two parts, which are local protection and pilot centralized protection. The local protection is designed for protecting the vulnerable power electronic components in converters and the pilot protection is mainly proposed for the fault isolation. The combination between two parts makes the whole system overcome the contradiction between protection speed and reliability and the method also takes the protection suitability into consideration. Finally, all the methods are verified by the simulation system based on the PSCAD /EMTDC.

Keywords: DC microgrid; system structure; local protection; centralized pilot protection

1. Introduction

The development of distributed generations (DGs) provides us with a valuable opportunity to utilize the electrical energy in a more environmentally-friendly way. For integration of DGs in power system, it is no doubt that the microgrid is a reasonable and effective technology. The DC microgrids, as a new form of microgrid, are attracting increasing interests all over the world. The less converter stages mean DC microgrids possess less grid losses than AC ones [1], and their control systems are much simpler, because there is no need to take the reactive power balance and frequency control into consideration [2]. In addition, the DC microgrids are more convenient and effective for DC loads, therefore, with the increasing of the DC loads, advantages of DC microgrids are becoming more and more remarkable [3].

However, the lack of mature protection schemes is a huge obstacle for development of DC microgrids [4,5]. One of serious issues is the contradiction between the system protection and control caused by system structures. The ring-bus structures are more reasonable for grid protection, because there are more than one power supply circuit, however, compared with single-bus structure system, the ring-bus system is not only complicated in structure but also difficult for the power flow calculation and power balance [6].

Furthermore, the protection system has its own troubles. At first, in a DC microgrid, there are usually a large number of converters for both the DGs and loads, while the vulnerable power electronics components in converters are only able to bear the overcurrent for less than 10 milliseconds [7,8]. Therefore, the speed requirements for protection are very rigid and not easy to be met.

What should be mentioned next is the existing methods of DCCBs (DC circuit breakers) installation [9], which are not appropriate for DC microgrids development.

As shown in Figure 1 [10], equipment needing three groups of DCCBs and two groups were installed in the bus, as a result, if there are large numbers of DGs and loads, the number of the expensive DCCBs would be huge, which means much more cost [11]. Meanwhile, when new equipment is needed to be added into a microgrid, four more CBs in the bus should be installed in bus, which is not beneficial for the system expansion and to be plug-and-play in future.

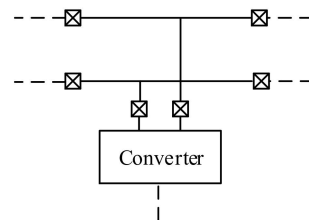


Figure 1. An existing DCCBs (DC circuit breakers) installation method in a DC microgrid.

Some protection methods have been proposed for DC microgrids. In [12], an event-based protection scheme was presented and has good performance, while, this scheme did not take characteristics of DGs into consideration. In [13], there was a protection strategy based on the local measurement, where the coordination between converters and bus contactors is employed to limit the fault current and isolate the fault. However, the strategy was only for medium-voltage DC microgrids and could not deal with large transient resistance well. A novel unit fault detection method based superimposed current was proposed in [14] for a single-bus DC microgrid. The method focused on cable and bus fault detection and did not involve the converters protection. In [15,16] protection methods for ring-bus DC microgrids are presented and both employed the conventional ring-bus structure (Figure 2b). Two methods were mainly proposed for VSC (Voltage Source Converter), therefore, they did not completely consider other converters.

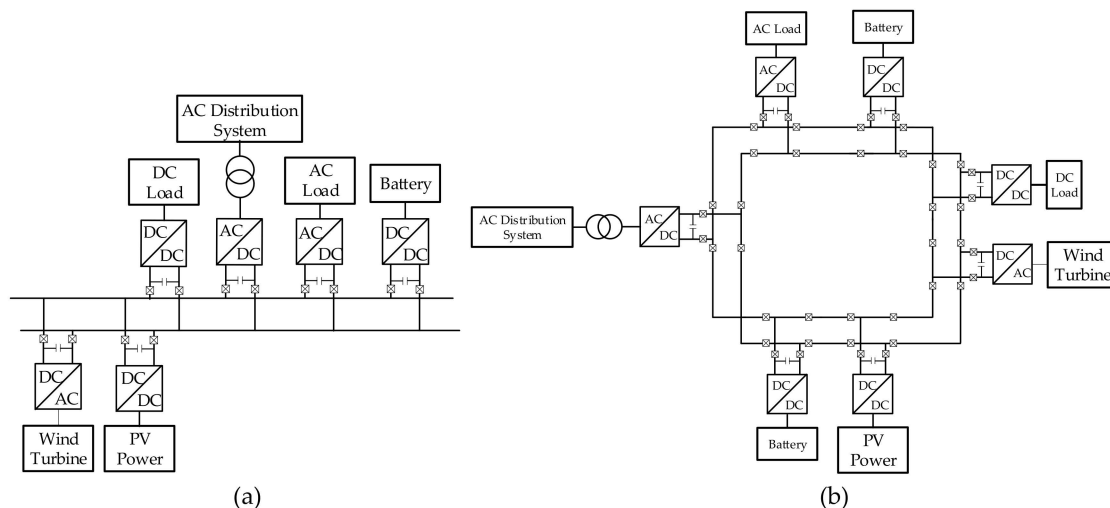


Figure 2. Two kinds of conventional DC microgrids. (a) The structure of a single-bus DC microgrid; (b) the structure of a ring-bus DC microgrid.

In this paper, an idea about DC microgrid structure is proposed at first, which can combine the advantages of both the conventional single bus and ring bus. Then, based on proposed structure, a protection system is designed, which includes a fast protection and a centralized pilot protection. The fast local protection is proposed for protecting the vulnerable power electronics components, which can meet speed requirements well. The pilot protection is mainly for the fault isolation, whose target is to detect and isolate the faulty zone accurately. The whole protection system is conventional for system expansion and equipment change and has great suitability for different converters.

This paper is divided into five sections. Section 2 introduces an idea to improve the system structure. In Section 3, local protection is illustrated, which is based on the fast fault current accumulative sum protection principle. Then, a centralized bus pilot protection strategy for isolating the faulty zone is proposed in Section 4. Finally, based on PSCAD/EMTDC, the simulation system is established and all the methods are verified in Section 5.

2. Structure of DC Microgrids

For the DC microgrids, the ring bus and single bus are the most common structures, whose typical structure are shown in Figure 2 respectively [17].

As mentioned above, the single-bus is a structure that is suitable for the control system but is not reasonable for the fault isolation, while, the ring-bus structure is opposite. The distribution grids usually have a structure of a ring-bus system and operate in single-bus state. Therefore, this idea is employed here to improve the DC microgrid.

The microgrid also has a ring-bus structure and the bus would be divided into several parts by the sectionalizing switches (SSes), which are all DCCBs. At least one SS remains open in order to avoid forming a ring electrically. An example system is presented in Section 5. Based on such a principle, the performance of the system control and protection can be balanced.

A protection zone in this structure is defined as a part of bus between two adjacent SSes. The DCCBs for one protection zone is shown in Figure 3. In this structure, the sectionalizing switches are not determined by operation states or equipment integration and the equipment are integrated into existing protection zones without changing the protection zones or SSes. As a result, the protection strategy based on this structure is more conventional and suitable for system expansion.

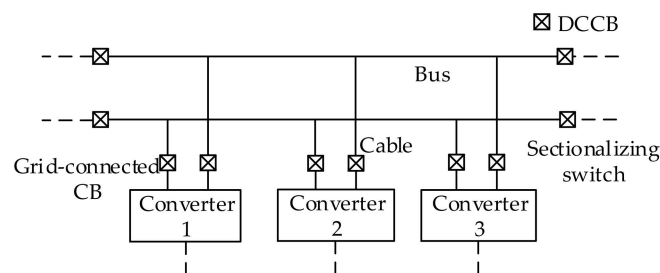


Figure 3. A protection zone in proposed structure.

3. Local Protection Method

3.1. Protection Targets and Fault Types Classification

The protection in this section is designed for protecting the equipment instead of clearing or isolating all the faults, as a result, the protection only needs to recognize and prevent the situation that may endanger its protection object. Therefore, this protection is only employed for grid-connected CBs and not for SSes.

During a serious fault, the controllable electric electronic components can be turned off by its self-protection immediately after fault, while the uncontrollable component would continue bearing the overcurrent and they are also easily damaged [18]. Those vulnerable devices should be the main protection objects, because only if they can avoid being damaged by faults, the converters can restart soon after fault is cleared.

Considering the damage caused by faults, the different kinds of faults have different impacts for vulnerable devices. Therefore, in this section, the faults are divided into three types, based on existing studies of DC system fault analysis.

For a grid-connected CB, a type 1 fault is the serious short-circuit faults occurring in its grid side (defined as external side), usually in a cable or bus. During such a fault, the fault characteristics are obvious, and the protection should operate in time to protect the equipment from the huge

overcurrent [19,20]. Normally, if an external fault leading to current peak reaches once bigger than load current, it can be seen as a type 1 fault [21].

Type 2 fault is the fault occurring inside the protection zone (defined as internal side), which means extremely short fault distance. When a type 2 fault occurs, the aim of protection is to isolate the protection range from the system immediately and satisfies that other parts of the system can operate normally [22]. However, the damage of the protected object is hard to avoid in such a case.

The type 3 fault is the fault occurring in an external system with a far distance or large transient resistance. Unlike type 1 and 2 faults, this kind of fault does not have clear characteristics and its destructive effect is very limited [23].

As a result, the protection does not need to operate very soon and there even may be no need to operate for a type 3 fault. Therefore, the type 3 fault should be treated differently from the type 1 and 2 faults. In this paper, the type 3 fault would be handled by the centralized pilot protection of Section 4.

3.2. Fault Current Accumulative Sum Protection

Based on the above analysis, for the faults of type 1 or 2, it is not hard to find that the main requirements for protection are the speed and reliability. The selectivity is not that important, because the protection only needs to discover threats and isolate the protected object from the system in time and it does not need to decide the fault location.

In this section, the protection based on fault current component is employed for type 1 and 2 faults, as the fault current component can reduce the interferences from the load current. The sampling points of fault current data ($I_f(k)$) can be calculated as follows,

$$I_f(k) = I(k) - I(k - N)(k > N), \quad (1)$$

where, $I(k)$ means a measurement data of current. N is equal to $T_c f_s$. T_c is calculation period. f_s is the sampling frequency of protection.

Based on the fault current calculated through Equation (1), a current accumulative sum protection method is proposed here. Compared with only adopting the fault current value directly, the accumulative sum can provide the protection with better speed and reliability. This accumulative sum current data ($I_{as}(k)$), can be calculated through Equation (2).

$$I_{as}(k) = \sum_{i=k-N+1}^{i=k} |I_f(i)|(k > N), \quad (2)$$

where, N is same with that of Equation (1).

The absolute value is employed in Equation (2), because the method would deal with both the current increasing and decreasing.

Then the protection operation equation is Equation (3).

$$I_{as}(k) > k_{rel} k_{cr} NI(k - N), \quad (3)$$

where, N is same with that of Equation (1), k_{rel} is the reliable coefficient and according to the existing protection experience, it can be 1.15–1.25. k_{cr} is the change rate coefficient. It can be seen that this operation equation means the average current variation exceeds k_{cr} times as large as load current during time T_c . For improving both the reliability and sensitivity, k_{cr} is normally 0.4–0.6, which is sensitive enough for the type 1 and 2 faults.

For the value of T_c , this period should be short enough, because a too long calculation period cannot effectively discover the current sudden change. However, a too short period is easy to be influenced by the load current fluctuating. Normally, the T_c is 2–5 ms in DC microgrids.

The accumulative sum can accelerate the protection, which means the more serious the fault is the faster the protection acts. Meanwhile, the method has a dynamic threshold, as a result, there is no

conventional setting value. Therefore, the protection suitability is improved, and complicated setting calculation is avoided.

4. Centralized Pilot Protection

The task of this protection is to detect and isolate the faulty zone and adjust the conditions of Sses after the fault is cleared. The pilot protection is employed here. A centralized protection also can be combined with proposed structure well, because the centralized protection possesses an obvious advantage of protecting the system from global perspective.

4.1. System Modeling

The topological information is the foundation for this centralized protection scheme, so it is necessary to number the protection zones and sectionalize switches at first.

The protection zone, which is connected with distribution system directly, is numbered as z_1 , and other zones should be named as z_2 to z_n successively in a clockwise direction.

For the sectionalizing switches, their current positive direction is also defined as clockwise direction. Their numbers are same with the adjacent protection zones located at their positive direction and are named as $s_1, s_2, s_3 \dots s_n$. This system modeling method is illustrated in Figure 4.

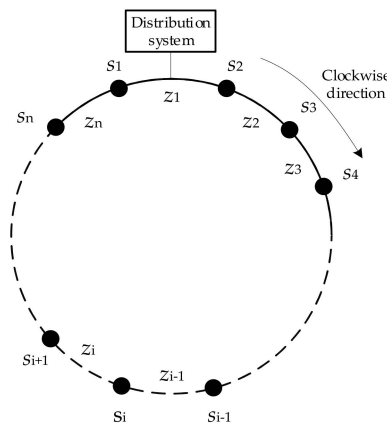


Figure 4. The modeling method for sectionalizing switches (Sses) and protection zones.

Besides, based on the numbers and current positive direction of positive pole, it is easy to create a current direction incidence matrix (matrix A). In this matrix, there are relations between the protection zones and current of their adjacent Sses. The forming principle of the matrix A is shown in Equation (4)

$$a_{ij} = \begin{cases} 1 & i = j, j = 1, 2, 3 \dots n \\ -1 & i = j + 1 (i = 2, 3, 4 \dots n, j = 1, 2, 3 \dots n - 1 \& i = 1, j = n) \\ 0 & \text{all else} \end{cases} \quad (4)$$

Matrix A is shown in Equation (5).

$$A = \begin{pmatrix} s_1 & s_2 & s_3 & s_4 & \dots & s_n \\ \begin{pmatrix} 1 & -1 & & & & \\ & 1 & -1 & & & \\ & & 1 & -1 & & \\ & & & \cdot & \cdot & \\ & & & & \cdot & \cdot \\ -1 & 0 & \cdot & \cdot & \cdot & 1 \end{pmatrix} & \begin{matrix} z_1 \\ z_2 \\ z_3 \\ \cdot \\ \cdot \\ z_n \end{matrix} \end{pmatrix} \quad (5)$$

4.2. Directional Element and Direction Information

The fault current direction information of the whole bus is necessary, so every position where SSES are installed should be a measurement point. For improving the protection reliability and sensitivity, all the directional elements include two parts, which are the starting element and the fault direction measurement element.

Based on the positive direction, the direction principle of fault current component is not hard to be established. For the positive pole, the positive fault current component means the positive fault. While, it is opposite for the negative pole. As a result, faulty pole selection is necessary for the directional element.

4.2.1. Directional Element for Grid-Connected CBs

For the grid-connected CBs, their directional elements are mainly based on the local protection of Section 3. Both the starting and fault direction are calculated through the fault current component. Their positive direction is defined as internal side and the microgrid side is the negative direction.

Those directional elements only send an internal fault message to the information center and block itself when there is a positive fault. They do not send any messages when there are external faults. A workflow for this directional element is shown in Figure 5.

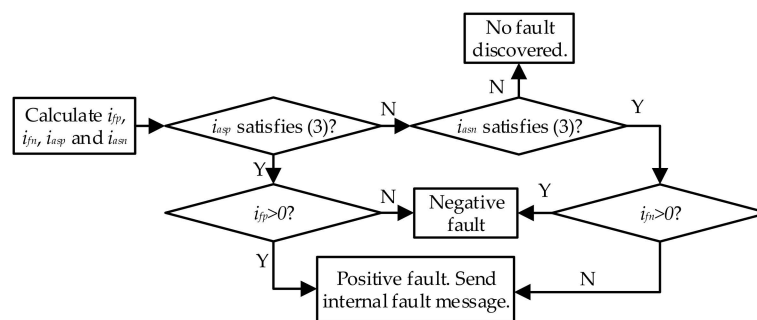


Figure 5. The flowchart for directional element of grid-connected CBs.

Where, i_{fp} and i_{fn} are fault current component of positive and negative pole respectively, which are both calculated through Equation (1). i_{asp} and i_{asn} are accumulative sum current from the positive and negative poles respectively, which are both calculated through Equation (2). It can be seen that this workflow has included the starting element, faulty pole selection, and direction measurement.

4.2.2. Starting Elements for the SSES

Unlike the local protection which only needs to deal with the dangers for the protected object, the pilot bus protection should be able to deal with all the faults, even the faults with very small fault current.

In addition, the pole-to-pole fault and pole-to-ground fault have different characteristics. The pole-to-pole faults are usually metallic and easy to be discovered, while, when it comes to the pole-to-ground-fault, they are usually the type 3 faults because of large transient resistance.

In this section, the starting elements have two algorithms of parallelism for two different faults and these are transverse differential algorithm and fault overcurrent algorithm.

Transverse differential current algorithm is proposed to deal with the pole-to-ground faults. The transverse differential current (i_{td}) is calculated through Equation (6)

$$i_{td} = i_p + i_n, \quad (6)$$

where the i_p and i_n are measurement current from the positive pole and negative pole respectively.

Based on the i_{td} , the pole-to-ground fault is easy to be discovered and the relative equation is Equation (7).

$$|i_{td}| > k'_{rel}k_{un}i_N, \tag{7}$$

where, k'_{rel} is also a reliable coefficient, which can be 1.15–1.25, according to the engineering experience; k_{un} is the unbalance current coefficient and its value can be 0.1–0.2, according to allowed maximum unbalance load current of a system. i_N is the nominal bus current.

The fault overcurrent algorithm is for the pole-to-pole fault, which is very simple and shown as follows.

$$|i_f| > k'_{rel}k_f i_N, \tag{8}$$

where, k'_{rel} is same with that of Equation (7). k_f is the fault current coefficient and can be 1.2–1.5. The i_f is fault current component and calculated through Equation (1).

The protection adopts the transient currents, which only occur when there are short-circuit faults, as a result, the normal load current fluctuating is not a threat anymore and protection has enough reliability itself. Therefore, the threshold can be properly declined to improve the protection sensitivity, which means the setting coefficient (k_{un} , k_f) can be a little smaller.

4.2.3. Direction Measurement Principle for the SSes

After the starting conditions are satisfied, the directional element would start. For the pole-to-pole fault, the first task of directional element is to find the faulty pole, because Equation (8) is only able to discover the fault. As the unfaultry pole current changes much less than that of faulty pole at the beginning of a fault, the faulty pole can be selected through Equation (9).

$$|i_{fp}| > |i_{fn}|, \tag{9}$$

where, i_{fp} and i_{fn} are the same with that of Figure 5.

If Equation (9) is satisfied, there is a positive pole fault and if not, the fault is negative pole pole-to-ground fault.

The direction data should be digital. In this paper, 1 is for the positive fault and -1 is for the negative fault. A 0 means the starting conditions are not satisfied and this data is set by the information center.

The complete workflow of this directional element is shown in Figure 6.

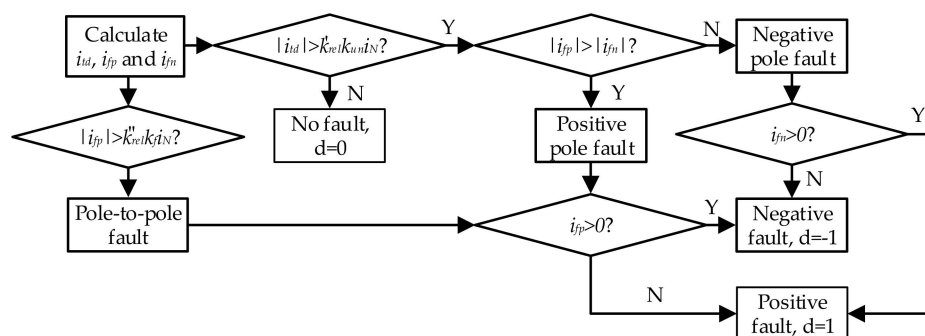


Figure 6. The flowchart for directional element of SSes.

4.3. Pilot Protection Algorithms

If the message sending conditions are satisfied, the direction information would be sent to the information center. After receiving the first direction information, the pilot protection starts, and the information center should wait for time t_d to receive all the information. The t_d can be determined by Equation (10)

$$t_d = t_{dmax} - t_{dmin}. \tag{10}$$

The t_{dmin} and t_{dmax} are the maximum and minimum normal delay time of communication system respectively. However, the directional elements of the open SSeS would not suffer any overcurrent; so, the information center should have a proper method for that condition.

At first, if the information center receives the internal fault message, the information center should send closing signals for all the equipment to recover the supply, while the blocked grid-connected CBs could not be closed by this signal.

If information center does not receive the block signal, the protection should calculate a result array to discover the fault zone further and direction array D is the foundation here.

In D , there are data for the direction information from the SSeS, and D_s is shown in Equation (11)

$$D = \begin{pmatrix} s_1 & s_2 & s_3 & \dots & s_n \\ d_1 & d_2 & d_3 & \dots & d_N \end{pmatrix}^T \quad (11)$$

where, the $d_1, d_2 \dots d_n$ means the direction information from the $s_1, s_2 \dots s_n$ respectively.

Then, a correcting matrix (matrix C) is proposed and the elements in correcting matrix can be created according to Equation (12).

$$\begin{cases} c_{ij} = -1/2 & d_{j+1} = 0, i = 1, 2, 3 \dots n, j = 1, 2, 3 \dots n - 1 \\ c_{ij} = -1/2 & d_{j-1} = 0, i = 1, 2, 3 \dots n, j = 2, 3, 4 \dots n + 1 \\ c_{ij} = 0 & \text{all else} \end{cases} \quad (12)$$

The correcting direction array (D'_s), is produced through Equation (13).

$$D' = CD. \quad (13)$$

Therefore, the final result array R can be obtained.

$$R = AD'. \quad (14)$$

If the element r_i in R satisfies $r_i > 1$, the z_i is the faulty zone.

The whole pilot protection flowchart is in Figure 7.

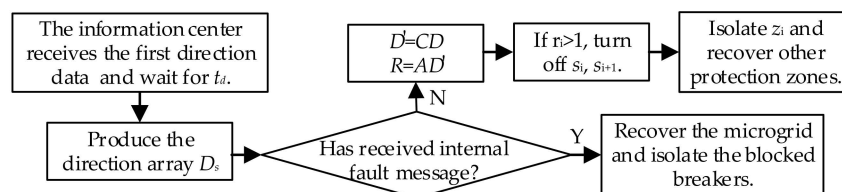


Figure 7. The flowchart of centralized bus pilot protection algorithms.

For the whole process, its main operation time is taken by t'_d and the simple calculation process only needs several milliseconds [24]. t'_d mainly depends on the communicated method and system size [25], which also can be less than 0.03 s for a microgrid, relying on existing technologies [26]. Therefore, the unfaulty equipment can restart in less than 0.05 s.

5. Case Study

The simulation system is established based on EMTC/PSCAD, which is shown in Figure 8 with the numbers of the protection zones (z_{1-4}) and SSeS (s_{1-4}). The protection zones of the bus are symbolled with different colors. It can be seen that compared with the systems in [15,16], the protection zones are much less. The f_{1-5} mean fault locations. The s_3 is set to be open at the beginning (marked by red) and other SSeS are closed. For the pole-to-ground faults, the positive pole is chosen as the faulty pole, and the pole-to-ground fault in the negative pole is symmetrical and possesses the same characteristics.

5.1. Simulation Results for Local Protection

In this section, effects of the fast protection method in Section 3 are tested. For simplifying the test, two typical converters, the VSC connected to distribution system and the PV (Photovoltaic) DC-DC converter in z_3 , are chosen as study objects.

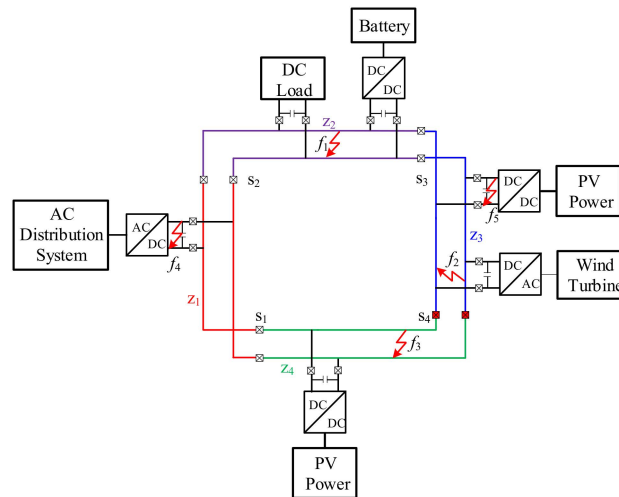


Figure 8. Simulation system.

The main parameters of the simulation system are illustrated in Table 1.

Table 1. The main parameters of simulation system.

| Voltage Stage | | DC-DC Converter Capacity | | VSC Capacity | Bidirectional DC-DC Converter Capacity | |
|-------------------|------------|--------------------------|--------|-------------------|--|-------------|
| 380 V | | 20 kW | | 50 kW | 10 kW | |
| Cable | | | | Bus | | |
| Resistance | Inductance | Capacitance | Length | Resistance | Inductance | Capacitance |
| 0.06 Ω /km | 0.28 mH/km | 0.3 mf/km | 200 m | 0.08 Ω /km | 0.32 mH/km | 0.4 mf/km |

For VSC, the f_2 and f_4 is adopted for simulation and faults in f_2 have a relatively long fault distance, which is the hardest situation for the protection. The faults in simulation consist of both the pole-to-pole fault and pole-to-ground faults with various transient resistances.

The protection parameters are shown in Table 2.

Table 2. The main parameters for local protection.

| k_{rel} | k_{cr} | T_c | f_s | N |
|-----------|----------|-----------------|---------------|-----|
| 1.2 | 0.5 | $2 * 10^{-3}$ s | $1 * 10^4$ hz | 20 |

Due to the difference between the pole-to-pole fault and the pole-to-ground fault, the simulation includes the five kinds of faults to completely test the protection performance. For type 1 and 3 faults, an external material pole-to-pole fault and pole-to-ground faults with 3 and 5 Ω transient resistances are adopted. Then, the type 2 fault includes a material pole-to-pole fault and a pole-to-ground fault with 5 Ω transient resistance. The DCCBs employs the SSCBs (Solid-State Circuit Breakers) [27] and their operation times are all set as 30 μ s [28]. The simulation results are shown in Figures 9–11, where the blue lines are the measurement current and the red ones are the operation current. The fault clearing times are show through purple lines. The unit of Y-axis is kA.

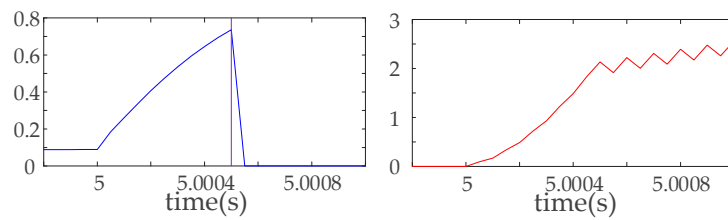


Figure 9. External pole-to-pole fault for Voltage Source Converter (VSC) protection.

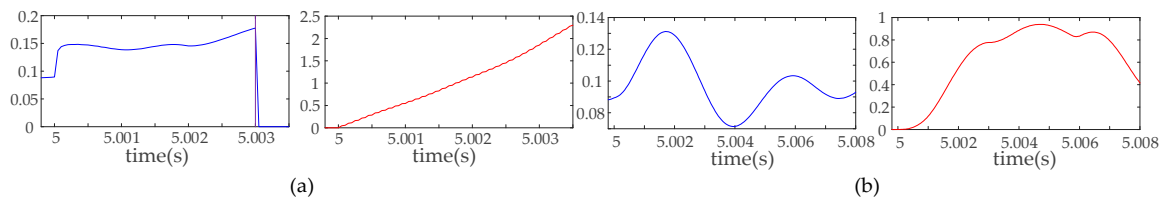


Figure 10. External pole-to-ground faults for VSC protection. (a) A 3 Ω transient resistance; (b) a 5 Ω transient resistance.

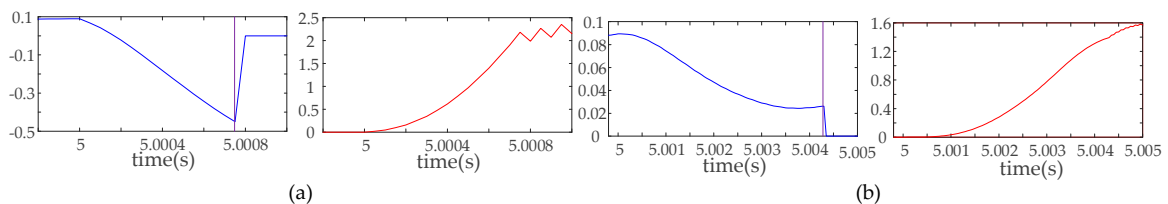


Figure 11. Internal faults for VSC protection. (a) Pole-to-pole fault; (b) pole-to-ground fault with 5 Ω transient resistance.

From Figures 9 and 10a, it can be seen that the protection reacts to the pole-to-pole and pole-to-ground fault with 3 Ω transient resistance rapidly. In Figure 10b, the protection does not operate because of a large transient resistance, while, it is also not hard to find that when the transient resistance is 5 Ω, the overcurrent peak just reaches 1.5 times the size of load current and only lasts for a short time. For the internal fault, the protection can deal with almost all of the situation even the large transient resistance, because of fast dropping current. In summary, the protection can protect the protected object fast and reliably.

For the PV power, the fault location is f_3 and f_5 , and the simulation employs the same kinds of the faults and protection parameters in the simulation for VSC protection. Performance of protection is shown in Figures 12–14, where the meaning of different colors is same with that of Figures 9–11. The unit of Y-axis is also kA. Obviously, the protection performance is similar to that of VSC protection, so there is no need to describe in detail again.

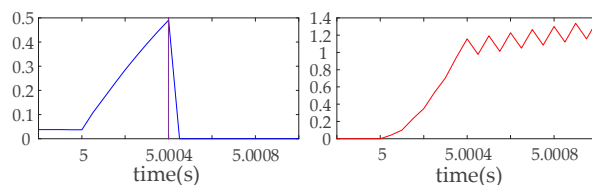


Figure 12. External pole-to-pole fault for Photovoltaic (PV) protection.

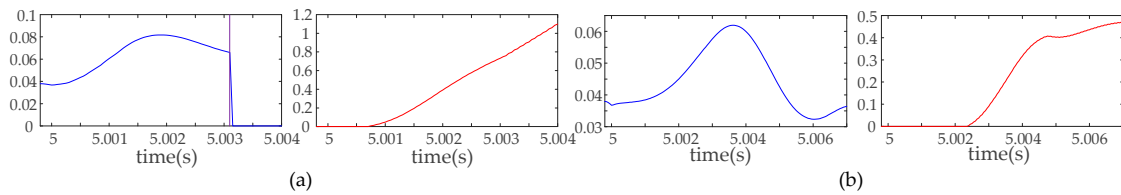


Figure 13. External pole-to-ground faults for PV protection. (a) A 3 Ω transient resistance; (b) a 5 Ω transient resistance.

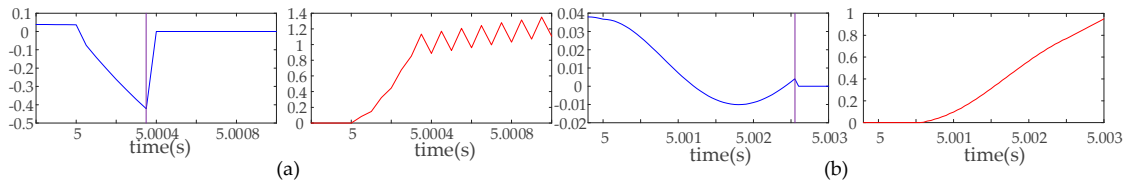


Figure 14. Internal faults for PV protection. (a) Pole-to-pole fault; (b) pole-to-ground fault with 5 Ω transient resistance.

Compared with existing methods that give specific operating times (Table 3), the proposed protection can handle the most serious faults in much less than 1 ms, as the accumulative sum effectively accelerates the protection. The protection can be adopted for different converters with the same parameters; therefore, protection has better suitability and can adapt to different working environments well.

Table 3. The operating time of different methods.

| Operating Time | | | |
|-----------------|-------------|-------------|-------------|
| Proposed Method | Method [12] | Method [13] | Method [15] |
| 0.38–3.5 ms | >5 ms | >10 ms | 1.8 ms |

5.2. Simulation Results for the Centralized Pilot Protection

When it comes to the centralized pilot protection in Section 4, the performance of the directional elements are verified at first. The fault location is chosen as location f_1 and f_2 . The relative protection parameters are shown in Table 4.

Table 4. The protection parameters for the centralized pilot protection.

| k'_{rel} | k_{un} | k_f | i_N |
|------------|----------|-------|--------|
| 1.2 | 0.15 | 1.3 | 0.1 kA |

The waveforms from the s_2 and s_3 are shown in Figure 15, which tests the performance of directional elements for the SSeS. The blue lines and red lines are the current from the s_2 and s_3 respectively. The purple means the protection thresholds, which are 0.156 kA for i_f and 0.018 kA for i_{td} . The negative protection threshold is for convenience of display, as Equations (7) and (8) both rely on absolute value. For the pole-to-ground fault, the transient resistance is 5 Ω and two waveforms in Figure 15d are totally coincident.

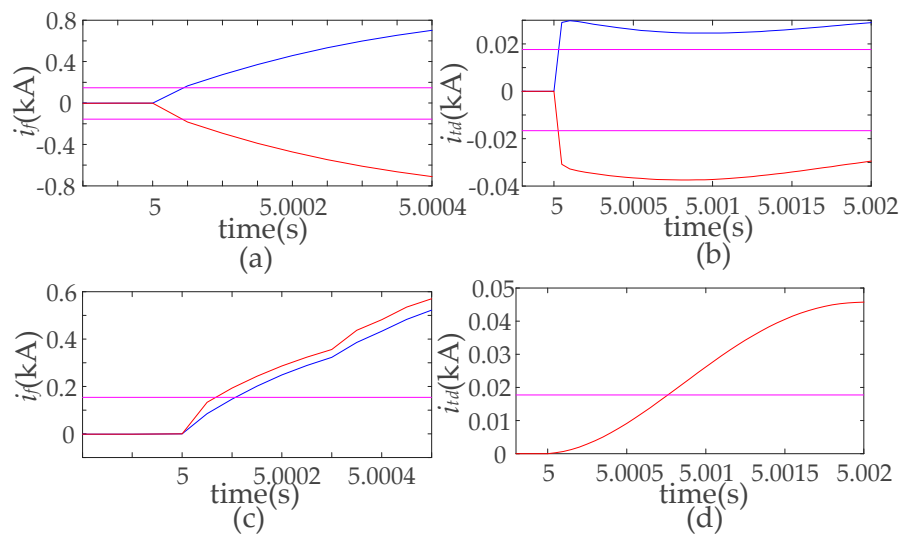


Figure 15. Transient current waveforms of s_2 and s_3 . (a) Pole-to-pole faults caused by f_1 ; (b) pole-to-ground faults caused by f_1 ; (c) pole-to-pole faults caused by f_2 ; (d) pole-to-ground faults caused by f_2 .

It is not hard to find the directional elements of centralized pilot protection have enough sensitivity and they are able to deal with large transient resistance. Based on the directions of i_f or i_{td} , it is obvious that the faults are forward faults for s_2 and backward fault for s_3 in Figure 15a,b. For Figure 15c,d, there are forward faults for both s_2 and s_3 . Therefore, for z_2 , Figure 15a,b, are obvious internal faults and Figure 15c,d are external faults.

The method in [16] is able to overcome very high transient resistance (10Ω), however, 5Ω is a high transient resistance for the DC microgrid, which is also employed in [14] and [15] and this simulation adopts much longer fault distance. Therefore, the protection has enough transient resistance tolerance ability.

Then, the pilot protection algorithms are tested, and the results are illustrated in Tables 5 and 6, where the bold numbers mean that this data meets the fault isolation conditions.

Table 5. Pole-to-pole fault simulation results for centralized pilot protection.

| Fault Location | D | D' | R | Results |
|----------------|--------------|--------------|-------------|---------------|
| f_1 | (1,1,-1,0) | (1,1,-1,0) | (0,2,-1,-1) | Isolate z_2 |
| f_2 | (1,1,1,0) | (1,1,1,-1) | (0,0,2,-2) | Isolate z_3 |
| f_3 | (-1,-1,-1,0) | (-1,-1,-1,1) | (0,0,-2,2) | Isolate z_4 |

Table 6. Pole-to-ground fault simulation results for centralized pilot protection.

| Fault Location | D | D' | R | Results |
|----------------|-------------|-----------------|-----------------|---------------|
| f_1 | (0,1,-1,0) | (-0.5,1,-1,0.5) | (-1.5,2,-1.5,1) | Isolate z_2 |
| f_2 | (0,1,1,0) | (-0.5,1,1,-0.5) | (-1.5,0,1.5,0) | Isolate z_3 |
| f_3 | (-1,-1,0,0) | (-1,-1,0.5,0.5) | (0,-1.5,0,1.5) | Isolate z_4 |

Through the result in the tables, it can be seen that all the fault zones can be detected, and protection is able to deal with both the pole-to-pole fault and pole-to-ground fault. Figure 16 shows the system structure changes for f_{1-4} , where red DCCBs are open ones. The protection can isolate and adjust the system correctly.

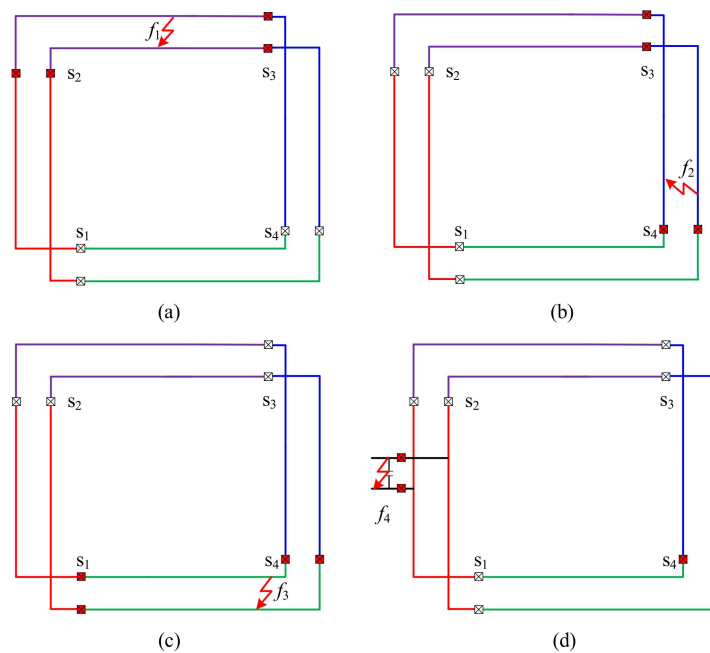


Figure 16. The protection isolation results. (a) f_1 faults; (b) f_2 faults; (c) f_3 faults; (d) f_4 faults.

6. Conclusions

In this paper, a complete protection system is established for an improved structure for DC microgrids. The main conclusions and shortages are as follows:

(1) In the future, there may be a large number of DGs and loads in a DC microgrid. This paper aims at proposing the structure and protection methods for such a system.

(2) The local protection and centralized pilot protection are responsible for the protection speed and selectivity respectively; as a result, both requirements can be satisfied.

(3) Some conventional overcurrent or inverse-time overcurrent backup protection can be adopted to avoid the possible load overcurrent for the converters, and it is not involved in this paper because of limited space.

(4) For recovering the whole system as soon as possible, distinguishing the transient fault and permanent fault is a very helpful way and this part can be researched in further studies.

Author Contributions: Formal analysis, Z.Z. and Y.Z.; Funding acquisition, Q.C.; Investigation, R.X. and Y.Z.; Project administration, Q.C.; Software, R.X.; Supervision, Q.C.; Writing—original draft, Z.Z.

Funding: This research was funded by the National Natural Science Foundation of China, grand number 51877123.

Conflicts of Interest: The authors declare no conflict of interest.

References

- Li, X.; Guo, L.; Wang, C. Key technologies of DC microgrids: An overview. *Proc. CSEE* **2016**, *36*, 2–17.
- Li, X.; Guo, L.; Li, Y.; Guo, Z.; Hong, C.; Zhang, Y.; Wang, C. A unified control for the DC–AC interlinking converters in hybrid AC/DC microgrids. *IEEE Trans. Smart Grid* **2018**, *9*, 6540–6553. [[CrossRef](#)]
- Liang, H.; Dong, Y.; Huang, Y.; Zheng, C.; Li, P. Modeling of multiple master–slave control under island microgrid and stability analysis based on control parameter configuration. *Energies* **2018**, *11*, 2223. [[CrossRef](#)]
- Zhang, L.; Chen, K.; Chi, S.; Lyu, L.; Cai, G. The Hierarchical Control Algorithm for DC Microgrid Based on the Improved Droop Control of Fuzzy Logic. *Energies* **2019**, *12*, 2995. [[CrossRef](#)]
- Aderibole, A.; Zeineldin, H.H.; Al Hosani, M.; El-Saadany, E.F. Demand Side Management Strategy for Droop-Based Autonomous Microgrids Through Voltage Reduction. *IEEE Trans. Energy Convers.* **2019**, *34*, 878–888. [[CrossRef](#)]

6. Wu, M.; Liu, H.; Chen, W. Research on active protection for MV/LV DC distribution system. *Proc. CSEE* **2016**, *36*, 891–899.
7. Zhao, Z.; Zhang, J.; He, Y.; Zhang, Y. Island DC Microgrid Hierarchical Coordinated Multi-Mode Control Strategy. *Energies* **2019**, *12*, 3012. [[CrossRef](#)]
8. Liang, H.; Huang, Y.; Sun, H.; Liu, Z. Research on Large-Signal Stability of DC Microgrid Based on Droop Control. *Energies* **2019**, *12*, 3186. [[CrossRef](#)]
9. Fletcher, S.D.A.; Norman, P.J.; Galloway, S.J.; Crolla, P.; Burt, G.M. Optimizing the roles of unit and non-unit protection methods within DC microgrids. *IEEE Trans. Smart Grid* **2013**, *3*, 2079–2087. [[CrossRef](#)]
10. Park, J.; Candelaria, J.; Ma, L.; Dunn, K. DC ring-bus microgrid fault protection and identification of fault location. *IEEE Trans. Power Deliv.* **2013**, *28*, 2574–2584. [[CrossRef](#)]
11. Salomonsson, D.; Söder, L.; Sannino, A. Protection of low-voltage DC microgrids. *IEEE Trans. Power Deliv.* **2009**, *24*, 1045–1053. [[CrossRef](#)]
12. Farhadi, M.; Mohammed, O.A. Event-Based Protection Scheme for a Multiterminal Hybrid DC Power System. *IEEE Trans. Smart Grid* **2015**, *6*, 1658–1668. [[CrossRef](#)]
13. Cairoli, P.; Dougal, R.A. Fault Detection and Isolation in Medium-Voltage DC Microgrids: Coordination Between Supply Power Converters and Bus Contactors. *IEEE Trans. Power Electron.* **2018**, *33*, 4535–4540. [[CrossRef](#)]
14. Mohanty, R.; Pradhan, A.K. A Superimposed Current Based Unit Protection Scheme for DC Microgrid. *IEEE Trans. Smart Grid* **2018**, *9*, 3917–3919. [[CrossRef](#)]
15. Mohanty, R.; Kumar, A.P. Protection of Smart DC Microgrid With Ring Configuration Using Parameter Estimation Approach. *IEEE Trans. Smart Grid* **2018**, *9*, 6328–6337. [[CrossRef](#)]
16. Mohanty, R.; Kumar, A.P. DC Ring Bus Microgrid Protection Using the Oscillation Frequency and Transient Power. *IEEE Syst. J.* **2019**, *13*, 875–880. [[CrossRef](#)]
17. Xue, S.; Qi, J.; Liu, C. A research review of protection for DC microgrid. *Proc. CSEE* **2016**, *36*, 3404–3412.
18. Szykiel, M.; Fletcher, S.; Burt, B.M. Electro-Thermal Analysis of Power Converter Components in Low-Voltage DC Microgrids for Optimal Protection System Design. *IEEE Trans. Smart Grid* **2018**, *9*, 5843–5846. [[CrossRef](#)]
19. Li, B.; He, J. DC fault analysis and current limiting technique for VSC-based DC distribution system. *Proc. CSEE* **2016**, *35*, 3026–3036.
20. Zhang, Z.; Chen, Q.; Xie, R.; Sun, K. The fault analysis of PV cable fault in DC microgrids. *IEEE Trans. Energy Convers.* **2019**, *34*, 486–496. [[CrossRef](#)]
21. Li, B.; He, J. Studies on the application of R-SFCL in the VSC-based DC distribution system. *IEEE Trans. Appl. Supercond.* **2016**, *26*, 1–5. [[CrossRef](#)]
22. Miao, Z.; Sabui, G.; Roshandeh, A.M.; Shen, Z.J. Design and analysis of DC solid-state circuit breakers using SiC JFETs. *IEEE J. Emerg. Sel. Top. Power Electron.* **2016**, *4*, 863–873. [[CrossRef](#)]
23. Yang, J.; Fletcher, J.E.; O'Reilly, J. Short-circuit and ground fault analyses and location in VSC-based DC network cables. *IEEE Trans. Ind. Electron.* **2012**, *59*, 3827–3837. [[CrossRef](#)]
24. Xia, Y.; Wei, W.; Peng, Y.; Yang, P.; Yu, M. Decentralized Coordination Control for Parallel Bidirectional Power Converters in a Grid-Connected DC Microgrid. *IEEE Trans. Smart Grid* **2018**, *9*, 6850–6861. [[CrossRef](#)]
25. Aluisio, B.; Dicorato, M.; Ferrini, I.; Forte, G.; Sbrizzai, R. Michele Trovato Optimal Sizing Procedure for Electric Vehicle Supply Infrastructure Based on DC Microgrid with Station Commitment. *Energies* **2019**, *12*, 1901. [[CrossRef](#)]
26. Wang, B.; Sechilariu, M.; Locment, F. Intelligent DC microgrid with smart grid communications: Control strategy consideration and design. *IEEE Trans. Smart Grid* **2012**, *3*, 2148–2156. [[CrossRef](#)]
27. Shen, Z.J. Ultrafast solid-state circuit breakers: Protecting converter-based ac and dc microgrids against short circuit faults. *IEEE Electrification Mag.* **2016**, *4*, 70–72. [[CrossRef](#)]
28. Wang, Y.; Li, W.; Wu, X.; Wu, X. A Novel Bidirectional Solid-State Circuit Breaker for DC Microgrid. *IEEE Trans. Ind. Electron.* **2019**, *66*, 5707–5714. [[CrossRef](#)]

